Topography dominates the hemispheric asymmetry of Stratospheric Sudden Warmings

Siming Liu[1], Tiffany Shaw[1], Chaim I. Garfinkel[2]

[1]Department of the Geophysical Sciences, The University of Chicago, Chicago, IL
[2]Fredy and Nadine Herrmann Institute of Earth Sciences, The Hebrew University of Jerusalem, Jerusalem, Israel

Key Points:

- Climate model simulations are used to quantify the impact of topography and ocean circulation on stratospheric sudden warmings.
- Topography is found to play a dominant role in shaping the hemispheric asymmetry of SSWs through its control on eddy heat flux.
- Topography amplifies eddy heat flux by increasing the amplitude of eddy meridional wind and temperature while decreasing their phase difference.

Corresponding author: Siming Liu, smliu01@uchicago.edu

Abstract

Stratospheric Sudden Warmings (SSWs) predominantly occur in the Northern Hemisphere with only 1 major event recorded in the Southern Hemisphere in the satellite era. Investigating factors that contribute to this asymmetry can help to reveal the cause of SSWs and lead to improved forecasts. Here we use climate model simulations to investigate the impact of boundary conditions (topography and ocean circulation) on the hemispheric asymmetry. Flattening topography eliminates Northern Hemisphere SSWs, while removing the ocean meridional overturning circulation reduces their frequency by half. The SSW response to boundary conditions is controlled by the hemispheric asymmetry of eddy heat flux. The reduction is driven by a decrease in amplitude of both eddy meridional wind and eddy temperature, as well as an increase in the cosine of the difference between their phases. The results suggest boundary conditions play an important role in shaping SSWs, especially topographic forcing, but that the boundary condition interactions are nonlinear.

Plain Language Summary

SSWs are powerful events that affect surface weather and climate. They mostly happen in the Northern Hemisphere, with very few occurring in the Southern Hemisphere. Understanding why this happens is important. Using climate model simulations, we quantify how boundary conditions, such as topography and ocean circulation, affect SSWs. The results suggest topography is the primary factor influencing the difference between hemispheres in SSWs. Topography is shown to control how much heat is transferred poleward by deviations from the zonal mean, which are known to drive SSWs. More specifically, flattening topography leads to changes in the wave phase and amplitude of meridional wind and temperature, which in turn causes a decrease in poleward eddy heat flux.

1 Introduction

Stratospheric Sudden Warmings (SSWs) represent abrupt disruptions in the winter stratosphere, characterized by rapid temperature increases and weakened or even reversed zonal-mean zonal winds in the polar vortex region (Butler et al., 2015; Baldwin et al., 2021; Qian et al., 2024). SSWs impact weather and climate in the Northern Hemisphere (NH) (Baldwin & Dunkerton, 1999) and Southern Hemisphere (SH) (Thompson et al., 2005), by shifting jet streams and storm tracks equatorward (Baldwin & Dunkerton, 2001; Afargan-Gerstman & Domeisen, 2020), inducing precipitation and temperature anomalies (Lehtonen & Karpechko, 2016; Lim et al., 2019). Additionally, for the SH, it suppresses strong heterogeneous ozone depletion, consequently impeding the formation of the ozone hole (Varotsos, 2002).

A notable feature of SSWs is the distinct hemispheric asymmetry in their occurrence (Krüger et al., 2005). The primary focus of SSWs has been on the NH, which occur with a frequency of slightly more than once every two years (Baldwin et al., 2021). In contrast, only one major SSW in the Southern Hemisphere (SH) took place in September 2002 (Allen et al., 2003; Simmons et al., 2005; Allen et al., 2006), and a minor one occurred in September 2019 (Hendon et al., 2019; Yamazaki et al., 2020; Rao et al., 2020).

One of the primary factors contributing to SSWs is the breaking of planetary-scale waves that propagate upwards from the troposphere (Matsuno, 1971), an important source of stratospheric variability (Polvani & Waugh, 2004; Cohen & Jones, 2011; Shaw & Perlwitz, 2013, 2014; Sjoberg & Birner, 2012, 2014; Dunn-Sigouin & Shaw, 2015, 2018, 2020). The weaker variability and fewer SSWs in the SH are attributed to weaker tropospheric wave driving (Plumb, 1989). Stationary planetary waves in the troposphere are triggered by various bottom boundary conditions (Held et al., 2002; Garfinkel et al., 2020), including large-scale topography (Charney & Eliassen, 1949), surface thermal forcing such as land-

sea contrasts (Smagorinsky, 1953) and asymmetric surface energy fluxes (Shaw et al., 2022), and the nonlinear interactions of synoptic-scale eddies (Scinocca & Haynes, 1998). Despite significant advances, the relative importance of these different forcings in driving stratospheric variability remains unclear.

Do all boundary conditions contribute equally to the asymmetry of SSWs, or does one dominate? Previous research has largely focused on idealized topography. Dry dynamical core models show that increasing the amplitude of idealized wave-2 topography promotes SSWs (Taguchi & Yoden, 2002; Gerber & Polvani, 2009; Sheshadri et al., 2015; Lindgren et al., 2018; Dunn-Sigouin & Shaw, 2018, 2020). Smaller topography amplitudes weaken the SH variability, while larger amplitudes enhance the NH variability. However, many studies neglect realistic topography with land effects.

Oceanic processes, such as the meridional overturning circulation (MOC), also influence stratospheric circulations by modulating planetary waves through sea surface temperature gradients (Hu et al., 2014). While White et al. (2017) examined localized topographic contributions to NH wintertime circulation, they did not consider other forcings, such as ocean processes. Similarly, Garfinkel et al. (2020) analyzed the role of various forcings in driving NH stationary waves but did not address how they contribute to the hemispheric asymmetry of SSWs. These limitations underscore the need to explore how different boundary conditions contribute to the hemispheric asymmetry of SSWs.

To address this, our study examines the relative contributions of boundary conditions, including realistic topography and surface energy flux over the ocean, to the hemispheric asymmetry of SSWs. Specifically, we aim to answer: (a) What are the relative contributions of boundary conditions to the hemispheric asymmetry of SSWs? (b) Through what mechanisms do boundary conditions affect stratospheric variability? We explore these questions using climate model simulations with modified surface (land and ocean) boundary conditions.

2 Data and Methods

2.1 Climate Model Simulations

We use ECHAM6 slab-ocean atmosphere general circulation model simulations previously reported by Shaw et al. (2022), which incorporates a realistic land surface featuring topography, a 50-meter mixed layer ocean depth, and prescribed monthly varying surface energy fluxes over the ocean quantified by the difference of NASA CERES TOA radiative flux and the atmospheric energy flux divergence derived from ERA-Interim reanalysis data (Frierson et al., 2013; Shaw et al., 2022). Similar results were found when using q-flux (the ocean heat flux) derived from a prescribed sea surface temperature simulation.

The impact of boundary conditions on SSWs hemispheric asymmetry is quantified by comparing 60-year simulations with realistic boundary conditions to those with flattened topography and symmetric surface energy fluxes. As discussed in Shaw et al. (2022), in the flattened topography experiment, surface geopotential and mean orography are set to zero. In the symmetrized surface energy flux experiment, surface energy fluxes are averaged across hemispheres, effectively removing the ocean meridional overturning circulation (Frierson et al., 2013) and east-west sea-surface temperature gradients.

2.2 Reanalysis

The ERA5 reanalysis (Hersbach et al., 2020) from 1958-2022 is used in this study. We used daily zonal and meridional wind and temperature to evaluate the model's ability to simulate a reasonable frequency of SSWs and eddy meridional heat flux.

2.3 SSW and Eddy Heat Flux Definitions

The identification of a major SSW in both hemispheres follows the method in Charlton and Polvani (2007), where a major SSW occurs when zonal mean westerlies at 60°N/60°S and 10 hPa reverse to easterlies for at least 3 days during winter (November-March for the NH, May-September for the SH). The wind reversal date is the onset date, and subsequent events within 20 days are excluded. SSWs where easterlies do not return to westerlies before April are also omitted.

To quantify wave activity entering the stratosphere, we calculate the monthly mean meridional eddy heat flux $\overline{v^*T^*}$ at 100 hPa (Polvani & Waugh, 2004), where v is the meridional wind, T is temperature, and the overline and asterisk indicate monthly means and zonal deviations. We also decompose v and T at 60°N and 100 hPa into wavenumbers, calculating the amplitude and phase of each wave component as per Watt-Meyer and Kushner (2018).

3 Results

3.1 SSWs in Climate Model Simulations

In ERA5, the frequency of SSWs per year (f_{SSW}) in the NH is approximately 0.61/year while there is only 1 major SSW in the SH, consistent with previous studies (Butler et al., 2015; Baldwin et al., 2021). The model with realistic boundary conditions, including observationally derived climatological surface energy fluxes (hereafter referred to as ALL), reproduces the observed f_{SSW} in the NH (Fig. 1a, ALL), outperforming most CMIP5/6 simulations (Rao & Garfinkel, 2021). It also accurately captures the hemispheric asymmetry in f_{SSW}, as no SSWs are simulated in the SH.

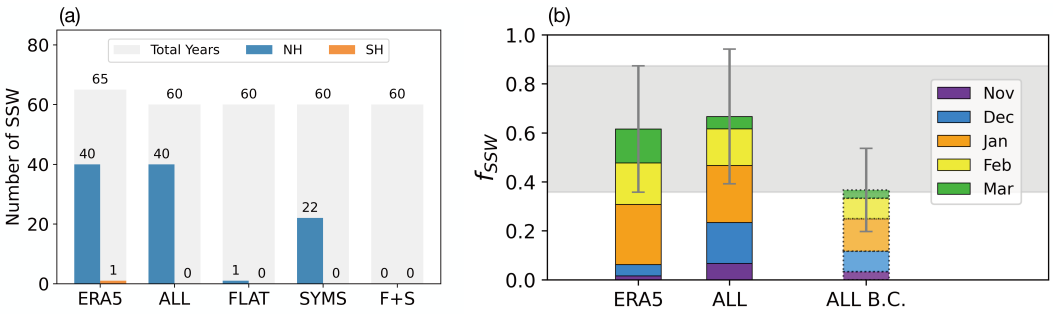

Figure 1. (a) Numbers of SSW in Northern (blue) and Southern (orange) Hemisphere in ERA5 reanalysis (1958-2022) and in the climate model simulations forced with realistic boundary conditions, including observationally derived climatological surface energy fluxes (ALL). Frequency of SSW is also shown for simulations with perturbed boundary conditions: flattened topography (FLAT), symmetrized surface energy fluxes (SYMS), and flattened topography and symmetrized surface energy fluxes (F+S). Grey bars in the background represnets the total length of the data. (b) Monthly distribution of the SSW frequency (f_{SSW}) in the NH of ERA5 (1958–2022) and climate model simulations (ALL). Each color-coded bar represents the percentage of years exhibiting an SSW in a given month. The third column is the bias corrected ALL (ALL B. C.) simulation where the daily zonal-mean zonal wind climatology at 10 hPa and 60°N (U_{1060}) is corrected by replacing it with ERA5. The gray shading represents the 95% confidence interval of ERA5 and the gray whisker on each bar represents the 95% confidence interval of each simulation.

No SH SSWs are simulated in the climate model, which may seem like a bias but is expected. Jucker and Reichler (2023) show that SSWs in the SH occur once every 62 years in a 9990-year coupled climate model simulation, making it plausible for no events to appear in a 60-year simulation.

To further assess the model's capability in simulating stratospheric variability, Fig. 1b illustrates the monthly distribution of SSW frequency in the NH. Unlike the common CMIP5/6 bias where SSWs peak in late winter (February-March) (Wu & Reichler, 2020; Rao & Garfinkel, 2021), the model's climatology simulation (ALL) places SSWs mainly in midwinter (January-February).

The simulated f_{SSW} can be affected by biases in the polar vortex mean state (Rao et al., 2019; Wu & Reichler, 2020). To address this, we apply a correction to align the model's mean state with observed values, generating an adjusted U_{1060} time series for detecting SSWs and calculating a refined f_{SSW}.

When the ALL simulation's zonal wind climatology at 10 hPa and 60°N is replaced with ERA5 values, f_{SSW} decreases (Fig. 1b, ALL B.C.), indicating an underestimation of U_{1060} (Fig. S1a,m). Despite biases in mean wind magnitude, the model effectively captures the vertical profile and seasonality of U_{1060} (Fig. S1). Both the original and corrected f_{SSW} remain within the 95% confidence interval of ERA5, outperforming many CMIP5/6 models, which often fall outside this range (Rao & Garfinkel, 2021). Thus, despite some discrepancies, the model is a strong tool for exploring SSW frequency under different boundary conditions (compare Fig. 1b to Fig. 2 in Rao & Garfinkel, 2021).

3.2 The Impact of Boundary Conditions on SSWs

Flattening topography in the model nearly eliminates SSWs in the NH and the hemispheric asymmetry, with only one SSW occurring in February (Fig. 1a, FLAT). When the model is forced with symmetrized surface energy fluxes, removing the ocean meridional overturning circulation, NH SSWs decrease by half (Fig. 1a, SYMS). With both flattened topography and symmetrized fluxes (Fig. 1a, F+S), no SSWs occur in either hemisphere during the 60-year simulation. These results suggest topography dominates the SSW hemispheric asymmetry, with a smaller contribution from ocean circulation, and that boundary conditions interact nonlinearly in affecting SSWs.

3.3 The Asymmetry of Meridional Eddy Heat Flux

To explain changes in SSW frequency, we examine the meridional eddy heat flux, which represents the upward propagation of tropospheric planetary waves. In ERA5, the NH eddy heat flux distribution at 100 hPa is positively skewed (Fig. 2a), with the ALL simulation closely replicating this pattern (Fig. 2b). The skewed distribution, particularly the long tail, implies that there is ample opportunity for internal variability to trigger strong planetary wave pulses that induce SSWs (Matsuno, 1971; Watt-Meyer & Kushner, 2018).

When topography is flattened (Fig. 2c, e), the median eddy heat flux decreases, reducing the likelihood of upward wave propagation and SSWs. Symmetrizing the surface energy flux (Fig. 2d) has a statistically insignificant impact on wave forcing based on K-S test, though NH SSW frequency drops by 1/3, with the median flux value falling from 7.13 to 6.66 Km/s and a 7% decrease in heat flux values above 10 Km/s. When both topography is flattened and fluxes are symmetrized (Fig. 2e), the median flux is significantly reduced, indicating topography is the dominant factor.

In the SH, with lower orography and fewer SSWs, the meridional eddy heat flux has a smaller median and fewer extremes (Fig. 2f, g). Flattening the topography slightly reduces the median heat flux, but the change is statistically insignificant (Fig. 2h). Symmetrizing surface energy flux also lowers the median heat flux (Fig. 2i, j). This is likely due to the

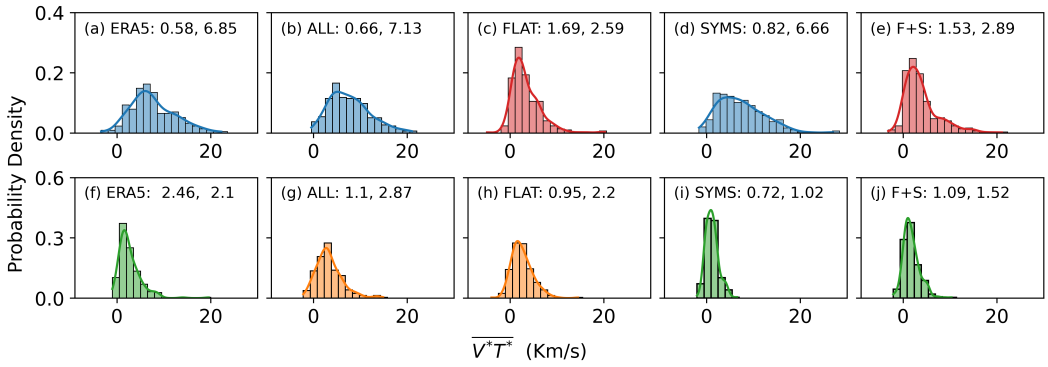

Figure 2. Distribution of the of monthly mean meridional eddy heat flux ($\overline{v^*T^*}$, Km s^{-1}) at 100 hPa averaged poleward of 45°N/S in the SSW related season (NH: Nov-Mar, SH: May-Sep) in (a)(f) ERA5 and (b)(g) ALL , (c)(h) FLAT, (g)(i) SYMS, and (e)(j) F+S simulations. The top row is for the NH and the bottom row is for Southern Hemisphere (heat flux values in the SH are multiplied by −1 for visual clarity). The value at the top of each panel are the skewness and median value of the distribution, respectively. Distributions that are significantly different from ALL (statistical significance at 95% level based on K-S test) have different colors.

predominance of oceanic areas in the SH, where applying symmetric surface energy flux average out the zonal differences, consequently weakening the stationary circulation.

We further examine the vertically-integrated spatial structure of the eddy heat flux. In ERA5, NH heat flux is large in the mid-latitudes, especially around 120°E, which is captured by ALL (Fig. S2a, d). In contrast, the SH shows smaller, less significant longitudinal flux structure(Fig. S2b, e). The simulation with topography highlights a strong NH asymmetry, especially near 120°E, downstream of the Tibetan Plateau, with a 40% extratropical asymmetry similar to ERA5's ∼ 50% (Fig. 3f).

When topography is flattened, this asymmetry drops to 3% across all longitudes, especially in the extratropics (Fig. 3c, e), consistent with the NH eddy heat flux reduction (Fig. 2c, e). The impact of topography on flux asymmetry is evident at multiple levels (850 hPa, 300 hPa, and 100 hPa, Fig. S3-5) and is most pronounced in the NH near significant topographic features (e.g., 120°E and 100°W), while the change in the SH is negligible.

In contrast, when surface energy fluxes are symmetrized, the eddy heat flux asymmetry is not significantly reduced (Fig. 3d), with the extratropical asymmetry still at 37% (Fig. 3f). Symmetrizing surface fluxes reduces meridional eddy heat flux in both hemispheres across all levels (Fig. S3h, S4h, S5h). Finally, when both topography is flattened and surface fluxes are symmetrized, the eddy heat flux asymmetry becomes negligible again (Fig. 3e), with the extratropical asymmetry dropping to 7% (Fig. 3f). These results indicate that boundary conditions interact nonlinearly in their impact on meridional eddy heat flux.

3.4 How Topography Drives Eddy Heat Flux Asymmetry

The simulations reveal that flattening topography exerts a dominant control on sudden stratospheric warmings (SSWs) and the hemispheric asymmetry of the meridional eddy heat flux. But how does topography drive this asymmetry of eddy heat flux?

As discussed by Chen (2005), both topography and surface energy flux force stationary waves through similar mechanisms, primarily governed by Rossby wave dynamics. However, the goal of this study is not to investigate how stationary waves are generated by different

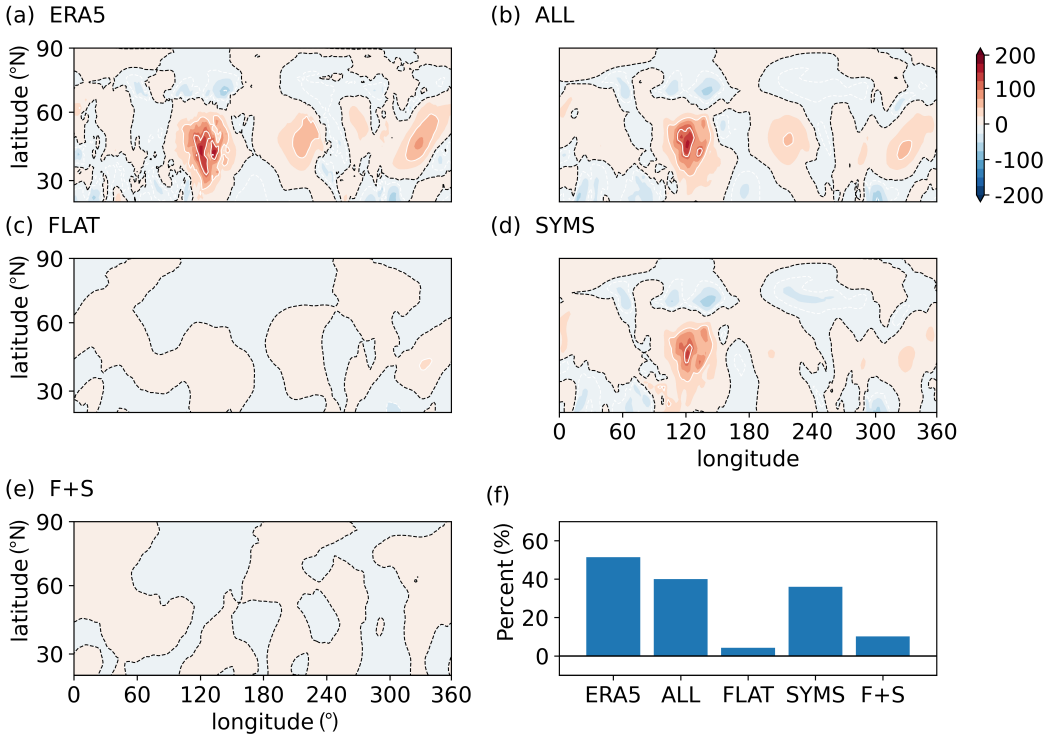

Figure 3. Difference of the amplitude of the vertically integrated monthly mean meridional eddy heat flux ($\overline{v^*T^*}$, Km s^{-1}) between Northern and Southern Hemispheres (heat flux values in the SH are multiplied by -1 for comparison) in SSW related season (NH: Nov-Mar, SH: May-Sep) in (a) ERA5, (b) ALL, (c) FLAT, (d) SYMS and (e) F+S simulations. The dashed black lines indicates where $\overline{v^*T^*}$ is equal to 0 Km s^{-1}. (f) Percentage difference of zonal-mean, vertically integrated stationary eddy heat flux ($\overline{v^*T^*}$, Km s^{-1}) (difference of the Northern and Southern Hemisphere divided by Northern Hemisphere) averaged over poleward of 20° across the simulations.

forcings. Instead, we focus on understanding how topography contributes to the occurrence of asymmetry in eddy heat flux.

Given the minor effect of topography on eddy heat flux distribution in the SH, we examines the changes in asymmetry when Northern Hemisphere (NH) topography is flattened. If v^* and T^* are represented using the complex exponential representation of a Fourier series, the absolute value of eddy heat flux $\left|\overline{v^*T^*}\right|$, which represents the alignment between two quantities, can be written as

$$\left|\overline{v^*T^*}\right| = \text{Real}\left\{A_v A_T e^{i(\theta_v - \theta_T)}\right\} = A_v A_T \left|\cos\left(\theta_v - \theta_T\right)\right| \tag{1}$$

where A_v and A_T are the amplitude of v^* and T^*, θ_v and θ_t are the phase of v^* and T^*.

Consequently, the decrease in $\overline{v^*T^*}$ when topography is flattened can result from: (1) a decline in amplitude of eddy meridional wind (A_v) and/or temperature (A_T); (2) a shift in the phase alignment between v^* and T^*, represented by $|\cos(\theta_v - \theta_T)|$, namely the two variables becoming out of phase. A cosine value of 1 indicates perfect alignment, while a value of -1 signifies opposite phases, both having an absolute value of 1. $|\cos(\theta_v - \theta_T)|$ decreases from 1 indicates the phase difference between v^* and T^* deviates from 0° (fully in phase) or 180° (completely out of phase).

Fig. 4 shows the probability distribution of the amplitude, and phase difference of monthly mean eddy meridional wind and temperature at 100 hPa and 60°N across the climate model simulations following Watt-Meyer and Kushner (2018). Flattening topography causes a statistically significant decrease of over 30% in the median wave-1 amplitude for both variables (Fig. 4a, b), with p values $\ll 0.01$ based on K-S test. Additionally, the phase difference between the two variables slightly increases (Fig. 4c), leading to a small decrease in the cosine of the phase difference (Fig. 4d).

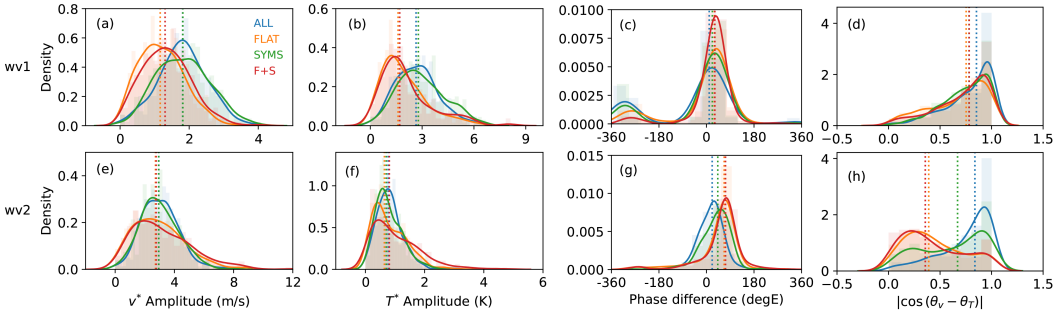

Figure 4. Probability distribution of the amplitude of monthly mean eddy meridional wind (v^*, m s^{-1}) (the first column) and monthly mean eddy temperature (T^*, K) (the second column), the phase difference between the two variables (the third column) and the cosine of the difference between their phases in the NH (the fourth column) for (a)-(d) wave-1 and (e)-(h) wave-2 component at 60°N and 100 hPa in SSW related season (NH: Nov-Mar) for ALL (blue), FLAT (orange), SYMS (green), and F+S (red) simulations. Solid curves represent Kernel Density Estimates for a smoothed visualization of the distributions, while histograms provide a discrete representation of the data. The dotted lines represents the median value for each distribution.

For the wave-2 component, the mode of the amplitude distributions decreases by over 20% when topography is removed (Fig. 4e, f) while the change in the median value is less significant compared to the wave-1 component. In contrast, the eddy meridional wind and temperature become more out of phase in the absence of topography (Fig. 4g). The phase difference increases by ∼40% following flattening topography, while the cosine of this difference decreases by roughly 60% (Fig. 4h), both of which are statistically significant (p values $\ll 0.01$, K-S test). This contributes to the reduction in NH eddy heat flux. Higher wavenumber components show an evident reduction in eddy temperature amplitude (Fig. S6b, f), while other variations remain relatively modest.

Overall, wave-1 heat flux reduction is due to decreased v^*, T^* amplitudes and increased phase difference, while the reduction in wave-2 median heat flux is driven mainly by phase difference.

To examine the effect of topography on eddy heat flux, we use a linear, quasi-geostrophic (QG) β-plane channel model to simulate stationary planetary wave motions in the middle atmosphere. The detailed equations, boundary conditions, and derivations are provided in the Supplementary Information. While the linear QG model cannot capture higher-order dynamics or the stationary wave field associated with other surface asymmetries, it can isolate the role of topography in modulating wave-mean flow interactions.

Supplemental Figure S8 shows that the topographic forcing in the QG model enhances wave amplitudes, eddy heat flux, and phase coupling between eddy meridional wind and temperature. Specifically, by comparing scenarios with realistic and smoothed topography, the figure demonstrates that reduced topography weakens wave amplitudes and increases

phase differences, consistent with results from ECHAM6 simulations and further bolstering the findings. Full results and comparisons are detailed in the Supplementary Information.

4 Discussion

This study used climate model simulations to quantify the impact of boundary conditions on the hemispheric asymmetry of SSWs. Our approach aligns with prior studies that used climate models to understand the impact of boundary conditions on the hemispheric asymmetry of atmospheric features (Manabe & Terpstra, 1974; Frierson et al., 2013; Shaw et al., 2022). More specifically, we quantified the impact of topography by flattening it, and the impact of the ocean meridional overturning circulation by symmetrizing the surface energy fluxes in the slab ocean (Stevens et al., 2013).

Our goal was to answer the two questions posed in the Introduction. Namely (1) What are the relative contributions of boundary conditions, including topography and the ocean meridional overturning circulation, on the hemispheric asymmetry of SSWs? (2) Through what mechanisms do boundary conditions affect stratospheric variability?

The answer to the first question is that topography dominates the hemispheric asymmetry of SSWs while the asymmetric surface energy fluxes plays a smaller role in the presence of topography. Topography essentially eliminates SSWs in the NH and eliminates the hemispheric asymmetry. Symmetrizing surface energy fluxes only reduces NH SSWs by 1/3. Notably, the impact of topography on the asymmetry percentage of eddy heat flux is substantial, exceeding 35%, with non-additive contributions from various boundary forcings indicating nonlinear interactions among them. Although our results demonstrate that the boundary conditions interact nonlinearly in terms of their impact on SSWs, it is clear that topography is the more significant factor.

The answer to the second question is that topography affects stratospheric variability by increasing the amplitude of eddy temperature and meridional winds, and decreasing their phase difference. Specifically, removal of topography results in a decrease in the median value of the amplitude for both eddy meridional wind and eddy temperature, particularly for wave number 1. This reduction is accompanied by an increase in the phase difference between the two variables, namely they becomes more out of phase with each other. These changes in both amplitude and phase induced by topography lead to a regional increase in eddy heat flux, especially over Eurasia, which indicates upward propagation of planetary waves into the stratosphere, thereby disturbing the polar vortex and causing more SSWs.

Our results are consistent with previous work that demonstrated topography significantly affects stationary wave features (Manabe & Terpstra, 1974; Held, 1983; Garfinkel et al., 2020). It is commonly assumed that both topography and land-ocean contrast contribute to the hemispheric asymmetry of SSWs and eddy heat flux. However, our analysis shows topography is the dominant factor.

Previous studies have shown that land-sea thermal contrast contributes to the generation of stationary waves (Garfinkel et al., 2020; Portal et al., 2022); however, our results indicate that its role in the asymmetry of SSWs is minor. While our simulations do not explicitly remove the impact of thermal forcing from land-sea contrast for direct comparison, its effect can still be observed in the flattened topography simulations (Figure S3d, e; Figure S10e, f). The results show that hemispheric asymmetry in eddy activity remains minimal when topography is removed, despite the presence of land-sea contrast. This suggests that stationary waves generated by land-sea contrast are weak and do not significantly contribute to the asymmetry, while topography exerts a more substantial influence. By flattening the topography, the contributions of both the topography and nonlinear interaction between topographic and thermal forcings are excluded, leaving only the minor contribution from thermal forcing. Reproducing these results in other climate models is important to ensure their robustness.

5 Data Availability Statement

The data analyzed in this study is available through Shaw et al., 2022.

References

Afargan-Gerstman, H., & Domeisen, D. I. (2020). Pacific modulation of the north atlantic storm track response to sudden stratospheric warming events. *Geophysical Research Letters*, *47*(2), e2019GL085007.

Allen, D. R., Bevilacqua, R. M., Nedoluha, G. E., Randall, C. E., & Manney, G. L. (2003). Unusual stratospheric transport and mixing during the 2002 antarctic winter. *Geophysical Research Letters*, *30*(12).

Allen, D. R., Coy, L., Eckermann, S. D., McCormack, J. P., Manney, G. L., Hogan, T. F., & Kim, Y.-J. (2006). Nogaps-alpha simulations of the 2002 southern hemisphere stratospheric major warming. *Monthly weather review*, *134*(2), 498–518.

Baldwin, M. P., Ayarzagüena, B., Birner, T., Butchart, N., Butler, A. H., Charlton-Perez, A. J., ... others (2021). Sudden stratospheric warmings. *Reviews of Geophysics*, *59*(1), e2020RG000708.

Baldwin, M. P., & Dunkerton, T. J. (1999). Propagation of the arctic oscillation from the stratosphere to the troposphere. *Journal of Geophysical Research: Atmospheres*, *104*(D24), 30937–30946.

Baldwin, M. P., & Dunkerton, T. J. (2001). Stratospheric harbingers of anomalous weather regimes. *Science*, *294*(5542), 581–584.

Butler, A. H., Seidel, D. J., Hardiman, S. C., Butchart, N., Birner, T., & Match, A. (2015). t. *Bulletin of the American Meteorological Society*, *96*(11), 1913-1928.

Charlton, A. J., & Polvani, L. M. (2007). A new look at stratospheric sudden warmings. part i: Climatology and modeling benchmarks. *Journal of climate*, *20*(3), 449–469.

Charney, J. G., & Eliassen, A. (1949). A numerical method for predicting the perturbations of the middle latitude westerlies. *Tellus*, *1*(2), 38–54.

Chen, T.-C. (2005). The structure and maintenance of stationary waves in the winter northern hemisphere. *Journal of the atmospheric sciences*, *62*(10), 3637–3660.

Cohen, J., & Jones, J. (2011). Tropospheric precursors and stratospheric warmings. *Journal of climate*, *24*(24), 6562–6572.

Dunn-Sigouin, E., & Shaw, T. (2018). Dynamics of extreme stratospheric negative heat flux events in an idealized model. *Journal of the Atmospheric Sciences*, *75*(10), 3521–3540.

Dunn-Sigouin, E., & Shaw, T. (2020). Dynamics of anomalous stratospheric eddy heat flux events in an idealized model. *Journal of the Atmospheric Sciences*, *77*(6), 2187–2202.

Dunn-Sigouin, E., & Shaw, T. A. (2015). Comparing and contrasting extreme stratospheric events, including their coupling to the tropospheric circulation. *Journal of Geophysical Research: Atmospheres*, *120*(4), 1374–1390.

Frierson, D. M., Hwang, Y.-T., Fučkar, N. S., Seager, R., Kang, S. M., Donohoe, A., ... Battisti, D. S. (2013). Contribution of ocean overturning circulation to tropical rainfall peak in the northern hemisphere. *Nature Geoscience*, *6*(11), 940–944.

Garfinkel, C. I., White, I., Gerber, E. P., Jucker, M., & Erez, M. (2020). The building blocks of northern hemisphere wintertime stationary waves. *Journal of Climate*, *33*(13), 5611-5633.

Gerber, E. P., & Polvani, L. M. (2009). Stratosphere–troposphere coupling in a relatively simple agcm: The importance of stratospheric variability. *Journal of Climate*, *22*(8), 1920-1933.

Held, I. M. (1983). Stationary and quasi-stationary eddies in the extratropical troposphere: Theory. *Large-scale dynamical processes in the atmosphere*, *127*, 168.

Held, I. M., Ting, M., & Wang, H. (2002). Northern winter stationary waves: Theory and modeling. *Journal of climate*, *15*(16), 2125–2144.

Hendon, H. H., Thompson, D., Lim, E.-P., Butler, A. H., Newman, P. A., Coy, L., & Scaife, A. (2019). Rare forecasted climate event under way in the southern hemisphere.

Nature, *573*(7775), 495–496.

Hersbach, H., Bell, B., Berrisford, P., Hirahara, S., Horányi, A., Muñoz-Sabater, J., ... others (2020). The era5 global reanalysis. *Quarterly Journal of the Royal Meteorological Society*, *146*(730), 1999–2049.

Hu, D., Tian, W., Xie, F., Shu, J., & Dhomse, S. (2014). Effects of meridional sea surface temperature changes on stratospheric temperature and circulation. *Advances in Atmospheric Sciences*, *31*, 888–900.

Jucker, M., & Reichler, T. (2023). Life cycle of major sudden stratospheric warmings in the southern hemisphere from a multimillennial gcm simulation. *Journal of Climate*, *36*(2), 643–661.

Krüger, K., Naujokat, B., & Labitzke, K. (2005). The unusual midwinter warming in the southern hemisphere stratosphere 2002: A comparison to northern hemisphere phenomena. *Journal of the atmospheric sciences*, *62*(3), 603–613.

Lehtonen, I., & Karpechko, A. Y. (2016). Observed and modeled tropospheric cold anomalies associated with sudden stratospheric warmings. *Journal of Geophysical Research: Atmospheres*, *121*(4), 1591–1610.

Lim, E.-P., Hendon, H. H., Boschat, G., Hudson, D., Thompson, D. W., Dowdy, A. J., & Arblaster, J. M. (2019). Australian hot and dry extremes induced by weakenings of the stratospheric polar vortex. *Nature Geoscience*, *12*(11), 896–901.

Lindgren, E., Sheshadri, A., & Plumb, R. (2018). Sudden stratospheric warming formation in an idealized general circulation model using three types of tropospheric forcing. *Journal of Geophysical Research: Atmospheres*, *123*(18), 10,125-10,139.

Manabe, S., & Terpstra, T. B. (1974). The effects of mountains on the general circulation of the atmosphere as identified by numerical experiments. *Journal of Atmospheric Sciences*, *31*(1), 3–42.

Matsuno, T. (1971). A dynamical model of the stratospheric sudden warming. *Journal of Atmospheric Sciences*, *28*(8), 1479–1494.

Plumb, R. A. (1989). On the seasonal cycle of stratospheric planetary waves. *Pure and applied geophysics*, *130*, 233-242.

Polvani, L. M., & Waugh, D. W. (2004). Upward wave activity flux as a precursor to extreme stratospheric events and subsequent anomalous surface weather regimes. *Journal of Climate*, *17*(18), 3548-3554.

Portal, A., Pasquero, C., D'andrea, F., Davini, P., Hamouda, M. E., & Rivière, G. (2022). Influence of reduced winter land–sea contrast on the midlatitude atmospheric circulation. *Journal of Climate*, *35*(19), 6237–6251.

Qian, L., Rao, J., Ren, R., Shi, C., & Liu, S. (2024). Enhanced stratosphere-troposphere and tropics-arctic couplings in the 2023/24 winter. *Communications Earth & Environment*, *5*(1), 631.

Rao, J., & Garfinkel, C. I. (2021). Cmip5/6 models project little change in the statistical characteristics of sudden stratospheric warmings in the 21st century. *Environmental Research Letters*, *16*(3), 034024.

Rao, J., Garfinkel, C. I., White, I. P., & Schwartz, C. (2020). The southern hemisphere minor sudden stratospheric warming in september 2019 and its predictions in s2s models. *Journal of Geophysical Research: Atmospheres*, *125*(14), e2020JD032723.

Rao, J., Ren, R., Chen, H., Liu, X., Yu, Y., Hu, J., & Zhou, Y. (2019). Predictability of stratospheric sudden warmings in the beijing climate center forecast system with statistical error corrections. *Journal of Geophysical Research: Atmospheres*, *124*(15), 8385–8400.

Scinocca, J., & Haynes, P. (1998). Dynamical forcing of stratospheric planetary waves by tropospheric baroclinic eddies. *Journal of the Atmospheric Sciences*, *55*(14), 2361–2392.

Shaw, T. A., Miyawaki, O., & Donohoe, A. (2022). Stormier southern hemisphere induced by topography and ocean circulation. *Proceedings of the National Academy of Sciences*, *119*(50), e2123512119. doi: https://doi.org/10.1073/pnas.2123512119

Shaw, T. A., & Perlwitz, J. (2013). The life cycle of northern hemisphere downward

wave coupling between the stratosphere and troposphere. *Journal of climate*, *26*(5), 1745–1763.

Shaw, T. A., & Perlwitz, J. (2014). On the control of the residual circulation and stratospheric temperatures in the arctic by planetary wave coupling. *Journal of the Atmospheric Sciences*, *71*(1), 195–206.

Sheshadri, A., Plumb, R. A., & Gerber, E. P. (2015). Seasonal variability of the polar stratospheric vortex in an idealized agcm with varying tropospheric wave forcing. *Journal of the Atmospheric Sciences*, *72*(6), 2248–2266.

Simmons, A., Hortal, M., Kelly, G., McNally, A., Untch, A., & Uppala, S. (2005). Ecmwf analyses and forecasts of stratospheric winter polar vortex breakup: September 2002 in the southern hemisphere and related events. *Journal of the Atmospheric Sciences*, *62*(3), 668–689.

Sjoberg, J. P., & Birner, T. (2012). Transient tropospheric forcing of sudden stratospheric warmings. *Journal of the Atmospheric Sciences*, *69*(11), 3420–3432.

Sjoberg, J. P., & Birner, T. (2014). Stratospheric wave–mean flow feedbacks and sudden stratospheric warmings in a simple model forced by upward wave activity flux. *Journal of the Atmospheric Sciences*, *71*(11), 4055–4071.

Smagorinsky, J. (1953). The dynamical influence of large-scale heat sources and sinks on the quasi-stationary mean motions of the atmosphere. *Quarterly Journal of the Royal Meteorological Society*, *79*(341), 342–366.

Stevens, B., Giorgetta, M., Esch, M., Mauritsen, T., Crueger, T., Rast, S., ... others (2013). Atmospheric component of the mpi-m earth system model: Echam6. *Journal of Advances in Modeling Earth Systems*, *5*(2), 146–172.

Taguchi, M., & Yoden, S. (2002). Internal interannual variability of the troposphere–stratosphere coupled system in a simple global circulation model. part i: Parameter sweep experiment. *Journal of the Atmospheric Sciences*, *59*(21), 3021-3036.

Thompson, D. W., Baldwin, M. P., & Solomon, S. (2005). Stratosphere–troposphere coupling in the southern hemisphere. *Journal of the atmospheric sciences*, *62*(3), 708–715.

Varotsos, C. (2002). The southern hemisphere ozone hole split in 2002. *Environmental Science and Pollution Research*, *9*, 375–376.

Watt-Meyer, O., & Kushner, P. J. (2018). Why are temperature and upward wave activity flux positively skewed in the polar stratosphere? *Journal of Climate*, *31*(1), 115-130.

White, R., Battisti, D., & Roe, G. (2017). Mongolian mountains matter most: Impacts of the latitude and height of asian orography on pacific wintertime atmospheric circulation. *Journal of Climate*, *30*(11), 4065–4082.

Wu, Z., & Reichler, T. (2020). Variations in the frequency of stratospheric sudden warmings in cmip5 and cmip6 and possible causes. *Journal of Climate*, *33*(23), 10305-10320.

Yamazaki, Y., Matthias, V., Miyoshi, Y., Stolle, C., Siddiqui, T., Kervalishvili, G., ... others (2020). September 2019 antarctic sudden stratospheric warming: Quasi-6-day wave burst and ionospheric effects. *Geophysical Research Letters*, *47*(1), e2019GL086577.